

Cheng Chen
Chen Peng
Hong Xiao
Tingyu Wang
Minjian Wei



<http://dx.doi.org/10.21278/brod73403>

ISSN 0007-215X
eISSN 1845-5859

NUMERICAL DISTRIBUTION SIMULATION OF TYPHOONS' WAVE ENERGY IN THE TAIWAN STRAIT AND ITS ADJACENT WATERS

UDC (265.578):551.466
Original scientific paper

Summary

As new energy technologies boom in recent years, marine renewable energy, especially wave power is one potential trend. However, few relevant studies focus on extreme sea conditions. In this paper, a numerical model of typhoon waves in the Taiwan Strait is established based on the third-generation ocean wave model SWAN and then calculated by the wave energy empirical equation. Typhoon No. 200808 Fung-wong, strong typhoon No. 200815 Jangmi and strong typhoon No. 201808 Maria are used for verification and analysis. Finally, the results show that most concentrated wave energy values are more than 300 kW/m for typhoon and more than 900 kW/m for strong typhoons, over 60 times and 180 times the annual average (5 kW/m) in the Chinese sea area, respectively. In terms of other locations, corresponding values are more than 50 kW/m and over 100 kW/m. Therefore, typhoons' wave energy is certainly a huge asset if fully utilized.

Key words: Taiwan Strait; Typhoon; SWAN model; Significant wave height; Wave energy

1. Introduction

Ocean is the naturally-endowed powerhouse to solve energy instability triggered by turbulent international situation. Marine renewable energy refers to the reusable power contained in waves, currents, tides and other forms in the marine environment [1]. Global scientists have carried out relevant studies on its schemes and efficiency, already gaining positive results.

According to references, In Denmark, a 110kW wave energy device had been tested for two years and another one with an installed capacity of 600kW was planned to be deployed in the Danish offshore wind farm [2]. Similarly in the United Kingdom, fourteen wave power units and five tidal power units with a total installed capacity of 7.6MW had been deployed and tested in southwestern England together with Pentland Firth and Orkney Islands, with extra 5 to 10MW array units on the way [3]. And in Germany, the University of Essen in Duisburg was developing a new wave and wind energy integration project, with a complete engineering

concept design and a future engineering prototype in 2014 [4]. One more case was another 120kW thermal wave energy demonstration project in Japan's Okinawa developed by the University of Tokyo to be put into operation in 2014. Relevant figures were 612m for water depth, 13000T for daily circulating water volume and 50~100kW of installed capacity [5]. Though being more complex than oil and gas mix in terms of structure analysis, offshore wind power can monitor and control machine loads, which indicates larger scope of progressive life-cycle strategies. Specifically, wave energy should focus on array optimization and cost reduction for large-scale manufacturing, deployment and operations [6-7].

According to World Meteorological Organization, a tropical cyclone with a sustained wind speed of magnitude 12 to 13 (32.7m/s to 41.4m/s) is defined as a typhoon or hurricane. Typhoons' movements are mainly affected by large-scale weather systems. They finally abate on the sea into extratropical cyclones, or disappear after landing. In the future, the wave power generation device to be set in the deep sea are more reliable to withstand larger waves generated by typhoons. Nowadays, wave and wind energy projects are in full swing globally. According to Liu et al. [8], China's tidal energy technology can rival the world's top, but diverges greatly with other ocean energy technologies, such as wave energy, temperature difference energy and salt difference energy. The mainstream ocean energy technologies are basically in the sea trial stage by proportional prototypes. Further equipment breakthroughs are needed to make better use of wave energy in Chinese waters, especially those generated by typhoons, as such energy can turn into strong powerhouse through technology advances rather than havoc and death.

Van et al. [9], Bento et al. [10], Rusu et al. [11], and Iglesias et al. [12] used the third-generation wave modes SWAN and WAVEWATCH III to simulate waves in their respective sea areas, and analyze significant wave height, wave energy density together with time and space distribution, so as to evaluate local wave energy resources. In this case, Europe's western coast owns top wave resources in the world due to its proximity to the Atlantic Ocean and the influence by strong storms. More specifically, the available wave energy in the northeast Atlantic Ocean (including the North Sea) is about 290 GW, and the average annual wave energy of the long period is about 25 kW/m in the southernmost Canary Islands, up to 75 kW/m in the waters off Ireland and Scotland [13]. Liu et al. [14], Wang et al. [15], Zheng et al. [16], Zhou et al. [17], and Qin et al. [18] conducted wave simulation of China's different sea areas through SWAN model, which showed rich wave energy in the northern and southern ends of the Taiwan Island, the southern sea area and southern Fujian Province. Besides, some scientists also had numerical simulation on extreme sea conditions [19] and a lot of typhoon-related work around this island. Chen et al. [20] evaluated the performance of significant wave heights modeling for typhoons on the northeastern coast of Taiwan using different wind fields and a fully coupled tide-surge-wave model. Hsiao et al. [21] quantified the contribution of nonlinear interactions to storm tide simulations during a super typhoon event. Liu et al. [22] investigated typhoon-induced storm surge and waves on the coast of Taiwan using an integrally-coupled tide-surge-wave model. However, few studies are available on wave energy distribution under extreme conditions such as typhoons despite higher wave in typhoon-affected areas and especially useful references for future relevant studies.

This paper mainly simulates three kinds of typhoons and calculates wave energy accordingly, then verifies model feasibility by wave energy at research points, finally calculating power volume and analyzing the space-time distribution. Next, the topics are simulation model in Section 2, research objects and areas in Section 3, the establishment and verification of the model in Section 4, along with simulation results and model accuracy in Section 5. Finally, Section 6 presents the main conclusions and suggestions.

2. Wind field model and wave model

2.1 Wind model

CCMP (Cross Calibrated Multi-Platform) sea surface wind field is the assimilation data of global surface wind field launched by NASA in 2009. It adopts the enhanced variational assimilation analysis combining relevant data collected on many oceans through passive microwave and remote sensing platforms of scatterometer. The CCMP wind field with high precision together with high spatial and temporal resolution are excellent for oceanic and atmospheric researches [23]. In this paper, the above-mentioned wind field is selected as the background in the driven wind field of the SWAN model [24-25]. The data comes from ESE (NASA Earth Science Enterprise) with a temporal resolution of 6h and a spatial resolution of $0.25^\circ \times 0.25^\circ$. In addition, ranges are from July 1927 to December 2020 for time, $78.375^\circ\text{S} \sim 78.375^\circ\text{N}$ for space, and from 180°W to 180°E for longitude.

The wind field calculation grid adopts a rectangular distribution, and the grid points are arranged as 131×131 . Its spatial resolution is $6' \times 6'$, distributed in the area of $17.625^\circ\text{N} \sim 30.625^\circ\text{N}$, $115.625^\circ\text{E} \sim 128.625^\circ\text{E}$. In the process of setting the SWAN model, white wave dissipation, wave breaking, bottom friction, nonlinear interactions and other physical processes are considered. Every calculation takes 6 hours.

2.2 Wave model

In the SWAN model, the random wave is represented by a two-dimensional dynamic spectral density: $N(\sigma, \theta) = E(\sigma, \theta) / \sigma$, where $N(\sigma, \theta)$ is the dynamic spectral density, and $E(\sigma, \theta)$ is the energy spectral density. In the spherical coordinate system, the energy balance equation can be expressed as:

$$\frac{\partial}{\partial t} N + \frac{\partial}{\partial x} C_x N + \frac{\partial}{\partial y} C_y N + \frac{\partial}{\partial \sigma} C_\sigma N + \frac{\partial}{\partial \theta} C_\theta N = \frac{S}{\sigma} \quad (1)$$

On the left, the first term refers to the change rate of action density over time, the second and third ones to the propagation of action density over geometric space, the fourth to the frequency shift due to water flow and changing depth, and the fifth to the effect of refraction and shallowing due to water flow and changing depth. S on the right side represents the energy source-sink, including wind energy input, white-hat dissipation, bottom friction, dissipation due to shallowing, three-wave interaction and four-wave interaction.

In the action balance equation, the headwind scheme determines the state. Therefore, a fully implicit finite difference scheme is adopted in SWAN model using a much larger time step than the explicit one in shallow water, so as to realize higher calculation accuracy [20].

3. Study objects and areas

In this paper, the three typhoons studied were divided into two groups according to wind scale [26], namely typhoon Fung-wong (200808) and strong typhoons Jangmi (200815) and Maria (201808). Their wave heights increased with higher typhoon level accordingly. Due to typhoons' long movement time and large calculation range, this paper mainly focuses on corresponding wave verification points and the wave energy characteristics during landing. Figure 1 shows moving paths of each typhoon.

Typhoon Fung-wong (200808) (see its route in Figure 1(b)) developed southeast of Ryukyu on July 25th, 2008, and moved towards northwest. It crossed the Taiwan Island and landed in China's Fujian Province at level 12, then weakening and disappearing towards northwest into Jiangxi Province, China. Fung-wong towards northwest, is one of the rare typhoons that still landed in Fujian Province after passing through Taiwan, heavily impacting southeastern coast of China.

On September 24th, 2008, Typhoon Jangmi (200815) (see Figure 1 (c)) formed over the western North Pacific and moved towards west by northwest. It crossed northern Taiwan that night and moved towards southwest briefly, rapidly weakening due to local topography into a severe tropical storm when leaving Taiwan on September 29th. Unlike Fung-wong, typhoon Jangmi didn't move across Taiwan but northwards to Japan.

Typhoon Maria (201808) (see Figure 1(d)) developed near Guam in the North Pacific Ocean. It moved towards northwest, weakened to a severe typhoon in eastern Taiwan, then moved further northwest. After landing in Huangqi Town in Lianjiang County, Fujian Province, China at 01:00 a.m. on July 11th, this typhoon gradually decreased in intensity and size, turning to northwest and eventually disappearing in Jiangxi Province of China.

Figure 1 shows typhoon routes. The thick solid lines stand for the coastlines, the thin solid lines for water depth isolines (unit: m), and location circles for typhoon centers at different time.

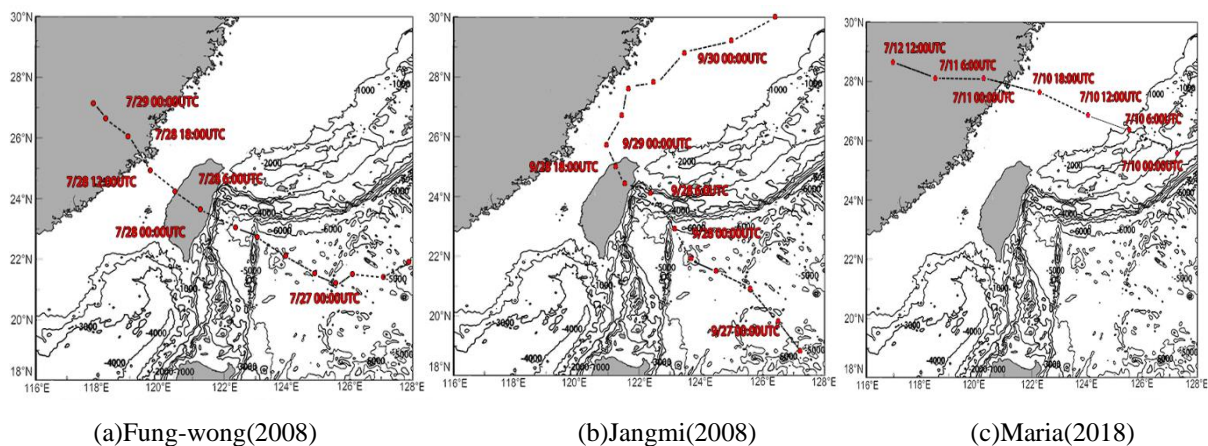


Fig.1 Track chart of typhoon

The bathymetry data used in the numerical simulation of research area is from ETOPO1 of NOAA (National Oceanic and Atmospheric Administration of the United States), and the topographic data is processed by the interpolation method. The scale range of this calculation was 18°N ~ 30°N, 116°E ~ 128°E, and the spatial resolution was 1'×1'. Water depth distribution is shown in Figure 2, which indicates that higher seabed topography gradually from inner to outer sea and deeper seabed as longitude and latitude rise. The maximum water depth reaches about 7500 m, comparing to that of less than 100 m in the Taiwan Strait.

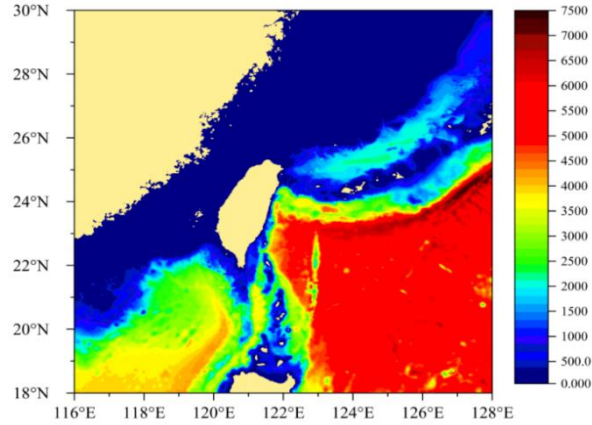


Fig.2 Bathymetric map

4. Model setup and validation

4.1 Model setup

4.1.1 Initial and boundary conditions

The SWAN model has land and water boundaries. According to its nature, the land boundary is further subdivided into three types: complete absorption, partial absorption and total reflection. The expression is as follows:

$$\frac{\partial \varphi}{\partial n} = ik \frac{1 - K_r}{1 + K_r} \varphi \quad \frac{\partial \varphi}{\partial n} = ik \frac{1 - K_r}{1 + K_r} \varphi \quad (2),$$

Where K_r is the reflection coefficient. Total reflection value is 1, total absorption is 0, and partial reflection ranges from 0 to 1. The water boundary mainly refers to that where the incident wave is. The boundary condition expression in SWAN is as follows:

$$\frac{\partial \varphi}{\partial n} = -p\varphi - q \frac{\partial^2 \varphi}{\partial \theta^2} + f \quad \frac{\partial \varphi}{\partial n} = -p\varphi - q \frac{\partial^2 \varphi}{\partial \theta^2} + f \quad (3)$$

Where $f = \partial \varphi_0 / \partial r + p\varphi_0 + q\partial^2 \varphi_0 / \partial \theta^2$, $p = [k^2 r^2 + k_0^2 r^2 + ik_0 r + 0.25] / [2ik_0 r^2]$, $q = 1 / [2ik_0 r^2]$, $\varphi_0 = \varphi_1 + \varphi_R$. Where φ_1 and φ_R represents the incident wave potential and the reflected wave potential, respectively. k_0 is the wave number on the open boundary.

To operate the SWAN model time-efficiently, a certain initial value will be selected from the previous results. Moreover, the time is calculated in advance to ensure more accurate output during early stage and outcomes.

4.1.2 Computational time step

In this paper, the wind field model of GEN3 is adopted in the scale of 18°N ~ 30°N and 116°E ~ 128°E, with the grid point arrangement of 145×145 and the spatial resolution of 5'×5'. Here the mesh is used to calculate the waves generated by the wind, while another one in the Section 2.1 is for the wind. What's more, a two-dimensional time-varying spherical coordinate system model is used. Its frequency range is 0.04 to 1.00 Hz, and the direction is divided into 24 segments with a resolution of 15°. The time step of model calculation is 15 minutes, delivering outcomes once per hour.

4.1.3 Wave energy calculation

Combining the background wind field with the typhoon wind field and introducing in the topographic height conversion equation as well, the synthetic wind field including terrain factor can be obtained, which can serve as the input data of the total typhoon wind field in SWAN model. The expression of the synthetic wind field [27] is as follows:

$$V_{hc} = (1-e)V_r \left(\frac{Z}{Z_c} \right)^\alpha + eV_{ccmp} \quad (4),$$

where V_{hc} is the synthetic wind field and V_r is the gradient wind field calculated by Holland equation. Z is related to the altitude of each point and Z_c to the altitude of the typhoon center. Moreover, α is the roughness coefficient of the ground, which adopts 0.16 according to the actual situation; V_{ccmp} is CCMP background wind field; e is the weight coefficient [28].

After debugging, $E = E_0 + 0.2$, $E_0 = \frac{C^4}{1+C^4}$, $C = \frac{r}{nR_{max}}$ are applied. In the equation, parameter n is 9 and weight coefficient e is:

$$e = \begin{cases} E & r \leq 3R_{max} \\ E + (1-E) * \frac{r-3R_{max}}{R_{max}} & 3R_{max} < r < 4R_{max} \\ 1 & r \geq 4R_{max} \end{cases} \quad (5),$$

where r is the distance from the point to the cyclone center for the grid calculate; R_{max} is the maximum wind speed radius, and the weight coefficient E is determined according to the distance between each grid point and the cyclone center. Hsiao et al. [29] found that when r increased from $4R_{max}$ to $7R_{max}$, the significant wave height of super typhoons in the deep sea also rose sharply. But in this study, the areas affected by typhoons were mostly in offshore waters. For example, when the distance between grid points and cyclone center is greater than or equal to 4 times the maximum wind speed radius, the model's input wind field is the background wind field.

Finally, the wave energy is calculated according to the empirical equation as follows [30]:

$$P = \frac{\rho g}{64\pi} H^2 T \approx 0.5 H^2 T P \quad (6),$$

where P is the wave energy, in kW/m; ρ is sea water density; g is the gravitational acceleration; H is the significant wave height; T is the wave period.

4.2 Model validation

4.2.1 Wave energy validation

The wave heights and wave periods generated by three typhoons are simulated, so as to calculate corresponding wave energy of each verification point in selected area. Then verifications are conducted by actual data, specifically, data of Suao Port (122°E, 24.30°N) in Taiwan's Yilan County for typhoon Fung-wong and typhoon Jangmi, and of Beishuang (120.3420°E, 26.694170°N) and No. 4 (120.7145°E, 26.2915°N) for typhoon Maria. Corresponding verification points are shown in Figure 3.

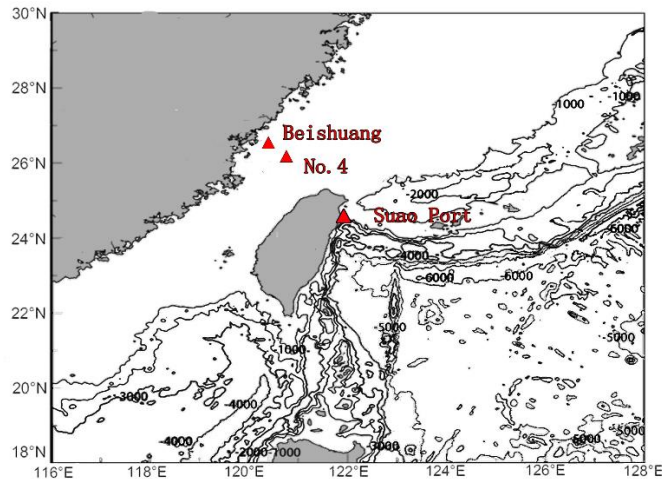
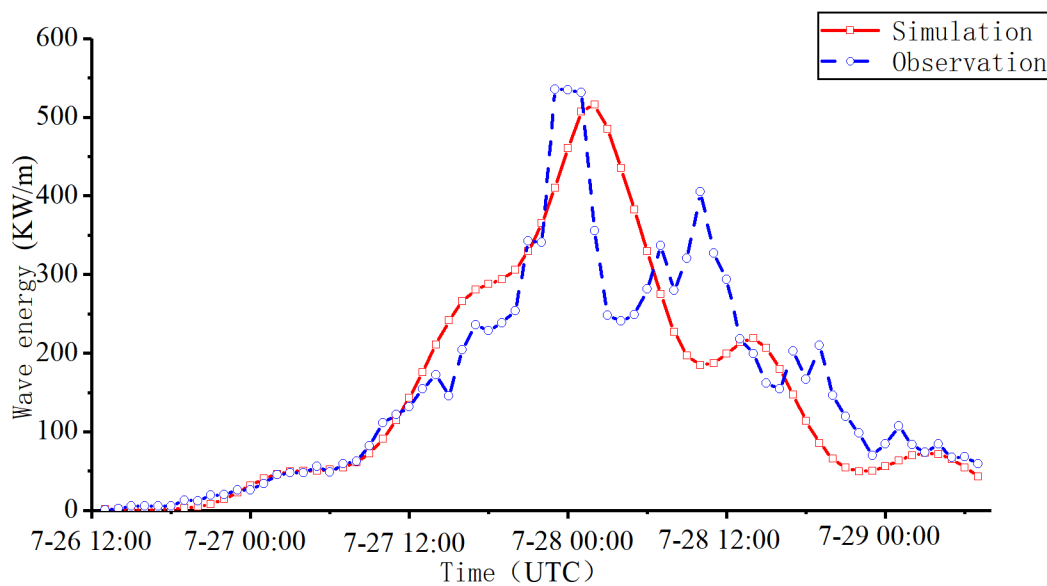
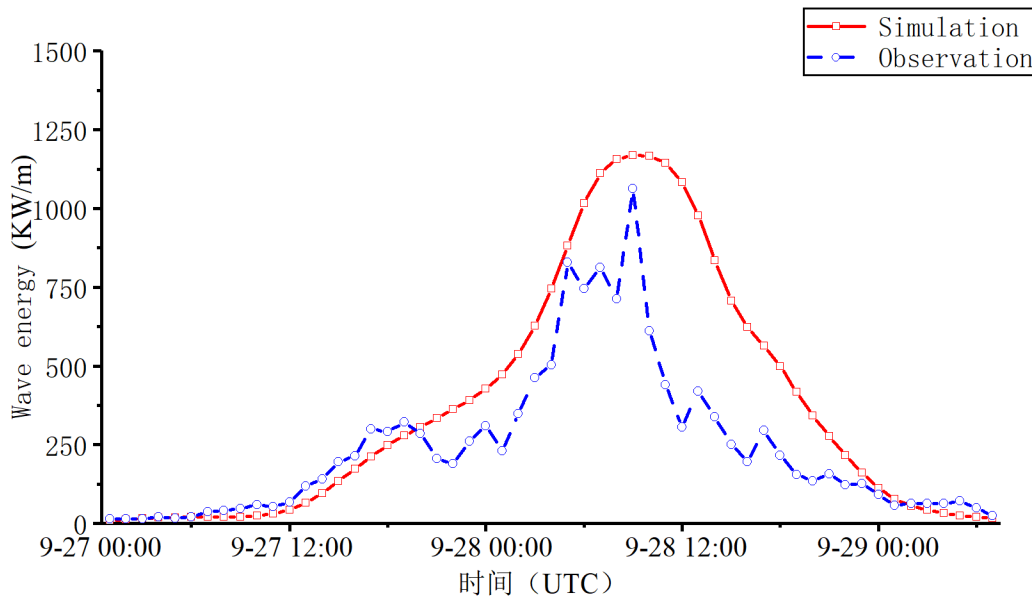


Fig.3 Location diagram of verification points

The wave energy of each verification point within the calculation range is shown in Figure 4. From it, there are deviations between calculated values and simulated results of both typhoon Fung-wong and typhoon Jangmi. Corresponding error of typhoon Fung-wong is 3% within a normal range, with a total error of 2%. The error of typhoon Jangmi between maximum wave energy and total wave energy was 9.8 % and 35.3 % respectively.



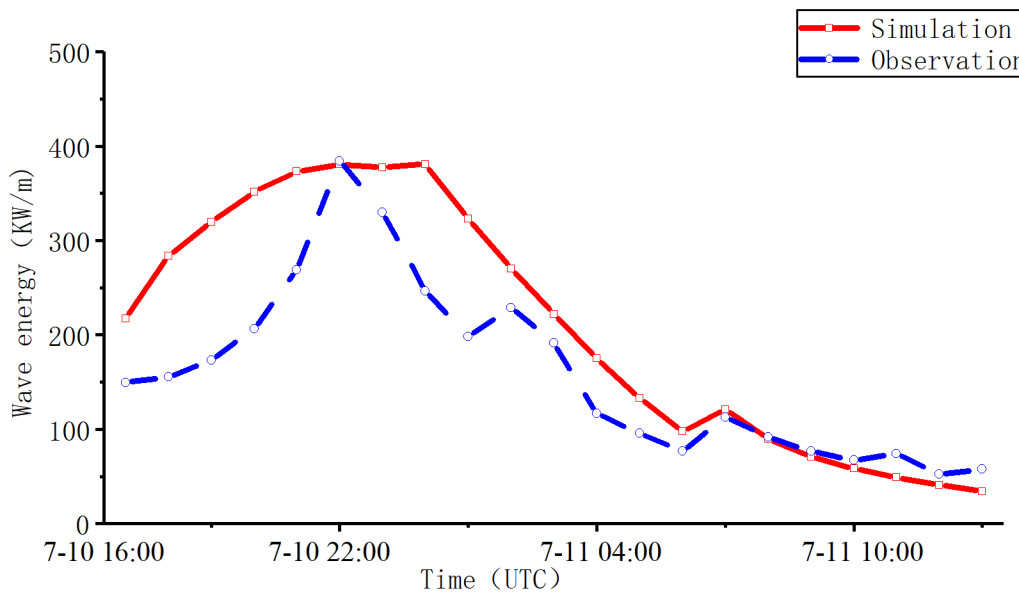
(a) Typhoon Fung-wong



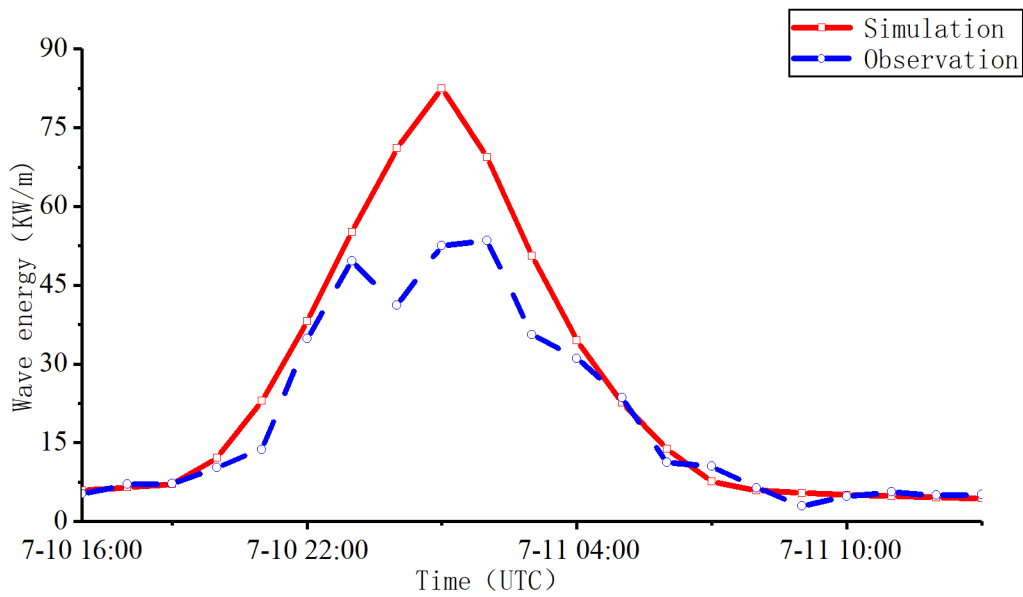
(b) Typhoon Jangmi

Fig.4 Comparison between calculated and observed wave energy at Suao Port

Figure 5 shows the wave energy in calculated time at verification point No. 4 and Beishuang, indicating that the calculated phase and simulation results are not highly consistent. The error of 1% between the maximum values at No. 4 is reasonable, while the total wave energy error is 25.3%. Namely, both errors are large at Beishuang's verification point.



(a) Verification point at No.4

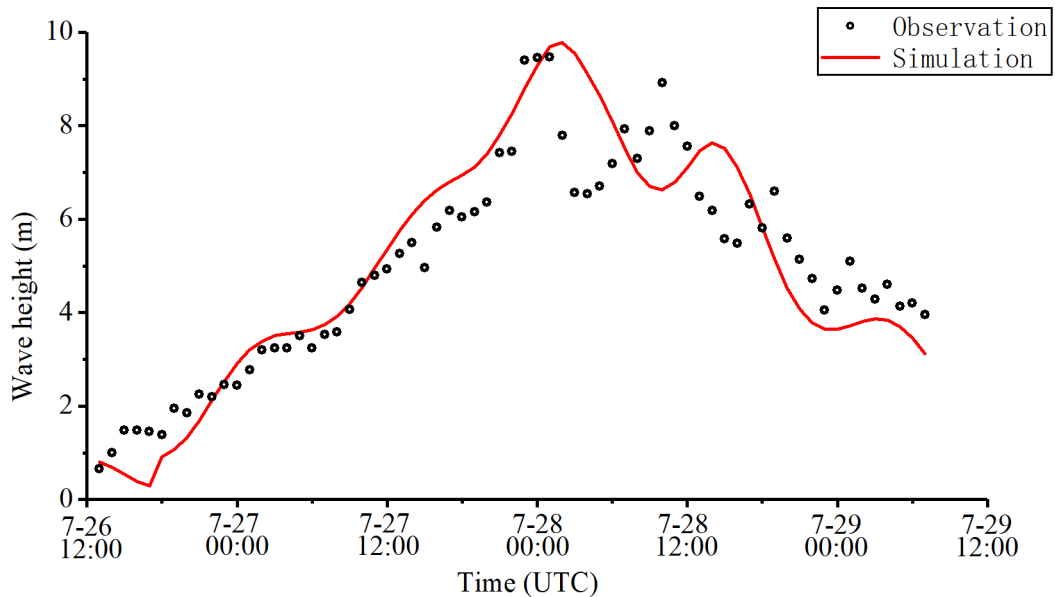


(b) Verification point at Beishuang

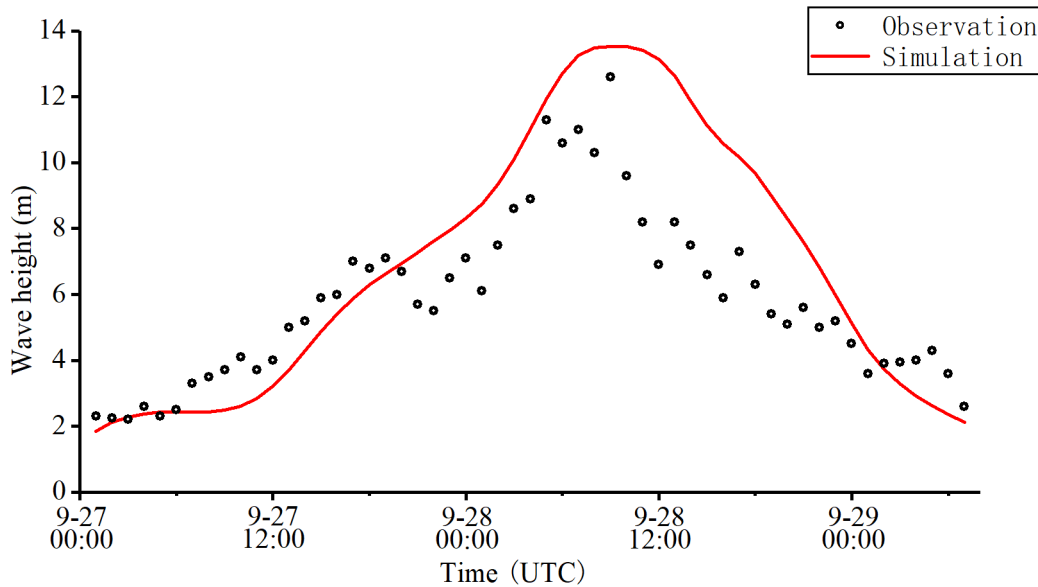
Fig.5 Comparison of calculated and observed wave energy of typhoon Maria

4.2.2 Significant wave height validation

Figure 6 and 7 compare between the measured and simulated values of the significant wave heights of typhoons Fung-wong, Jangmi and Maria at each verification point. The simulated values are in good agreement with the measured data, which indicates simulation feasibility and accuracy.

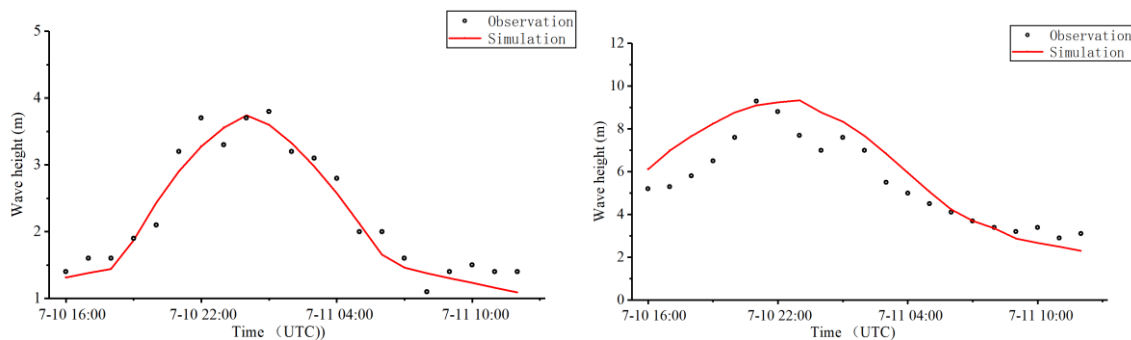


(a) Fung-wong



(b) Jangmi

Fig.6 Comparison of calculated and observed wave height of typhoon Fung-wong and Jangmi at Suao Port.



(a) Verification point Beishuang

(b) Verification point No. 4

Fig.7 Comparison of calculated and observed wave height of typhoon Maria

5. Numerical results and discussions

5.1 Wave energy distribution

Figure 6 (a) and (b) show the wave energy distribution and direction distribution of typhoon Fung-wong when it landed near Hualien, Taiwan. From these figures, when the typhoon landed, the wave energy was small on the left and large on the right, gradually decreasing from inside typhoon center to outside. The reason is that, affected by northern hemisphere's earth rotation angular force, the wind in the study area is shifting to the right, resulting in wind asymmetry along typhoon path, namely weaker on the left and stronger on the right. As wind is the major factor to generate waves, there is a positive correlation between wind and waves. This phenomenon corresponds to the regularity of tropical cyclone field in the northern hemisphere, the same as the significant wave height distribution. The wave energy peaks to 780 kW/m and greater than 50 kW/m in other regions, which is more than 10 times higher than the annual average value of 5 kW/m in the most concentrated wave energy distribution area around mainland China's sea areas.

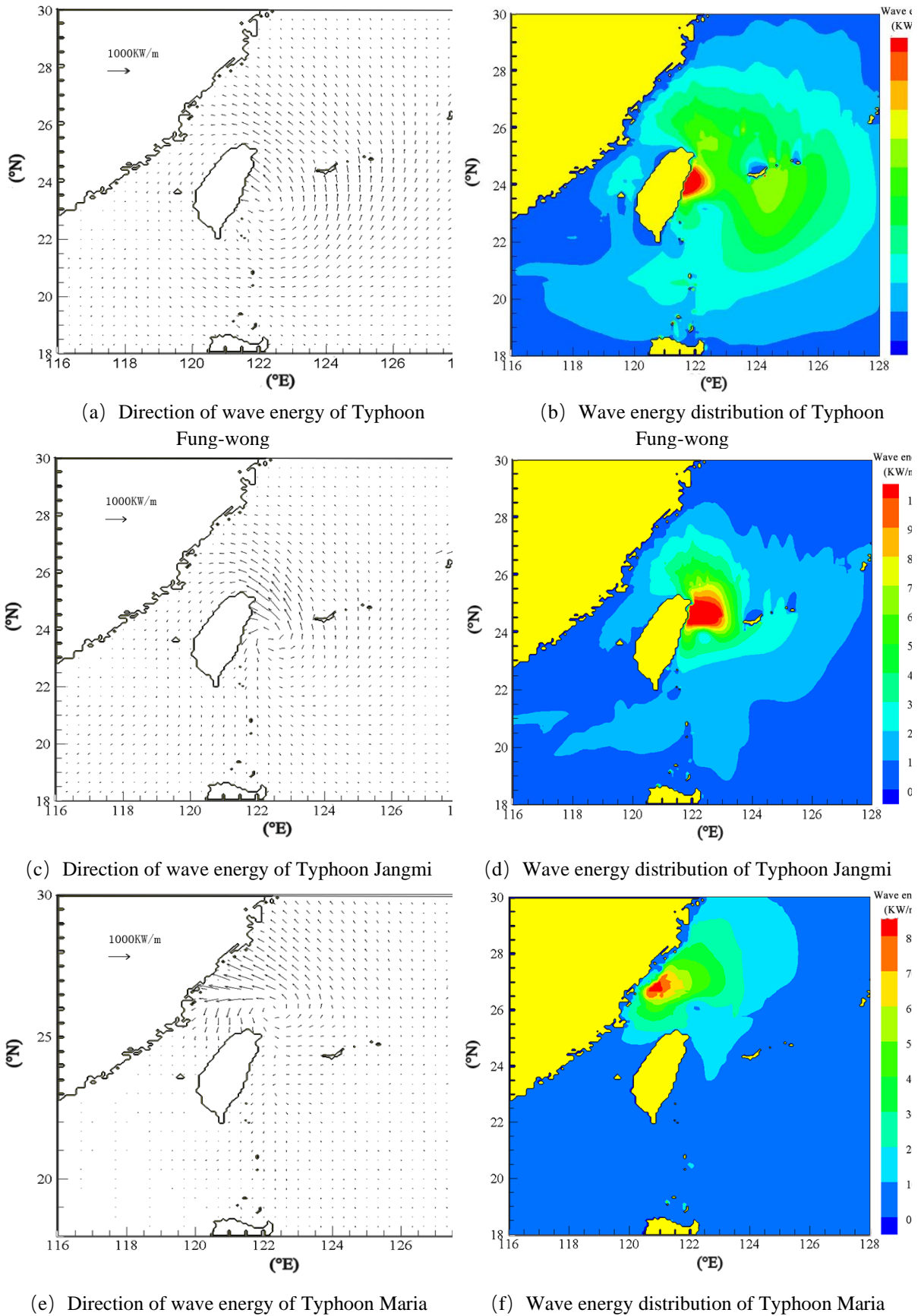


Fig.8 Direction and distribution of wave energy at typhoon landing time

According to Figure 6 (c) and (d), when typhoon Jangmi landed near Suao Port, Taiwan, the maximum wave energy reached 1321 kW/m towards 29.8° northeast. Most wave energy in other regions was greater than 100 kW/m, which was more than 20 times higher than the annual average value of 5 kW/m in the region with the most concentrated wave energy distribution in mainland China.

In terms of Figure 6 (e) and (f) as typhoon Maria landed near Ningde City, Fujian Province of China, the maximum wave energy reached 918 kW/m and greater than 100 kW/m in other regions, more than 20 times higher than the annual average volume of 5 kW/m in the region with the most concentrated wave energy distribution in mainland China.

5.2 Discussions

Figure 4 shows that typhoon Fung-wong's wave energy at Suao Port is about 500 kW/m, while that of typhoon Jangmi is about 1000 kW/m. This is because Jangmi is closer to the landing site of Suao Port and gradually grew stronger before landing while Fung-wong was already in the decreasing stage. Therefore, typhoon Jangmi reached its maximum wind speed near Suao Port, but Fung-wong did not. This explains why Jangmi had more powerful wave energy.

According to Figure 5, the total values of wave energy vary greatly. Due to accidental factors, measured values drop suddenly, while simulated ones show a slow and regular drop. In addition, when calculating the wave energy, the error is doubled due to the large waves formed by the strong typhoon, so there is a certain gap in the sum.

According to Figure 6 and 7, the significant wave heights at each verification point have the same trend and same peak time. However, there are still gaps between the simulated values and the measured ones. It is because that tides are not considered, which will be added to the simulations in the future.

There are errors in Figure 4-7, possibly because the terrain of the model is not accurate enough, resulting in different water depth from the actual one, or because the wave energy calculation equation used in this paper is more suitable for shallow water. In reality, both shallow water and deep water waves will be affected by typhoons.

6. Conclusions and suggestions

In this paper, three typhoons are divided into two groups according to intensity, including typhoon Fung-wong (200808) along with strong typhoons Jangmi (200815) and Maria (201808). These typhoons are simulated in SWAN mode to get wave heights and wave periods, then wave energy is calculated and verified by measured data. Corresponding results are as follows:

(1) Typhoon's maximum wave energy is more than 300 kW/m, 60 times higher than the annual average value (5 kW/m) of the most concentrated wave energy area in mainland China's sea area, and more than 50 kW/m in other locations in the region.

(2) For strong-typhoons, most of their wave energy in the maximum region is above 900 kW/m, 180 times higher than the annual average volume in the most concentrated wave energy area within mainland China's sea range, and more than 100 kW/m in other places in this region.

(3) The results show that the wave energy generated by typhoon is several times stronger than that under normal climate conditions. If properly utilized, it is a substantial new energy treasure house to be further developed.

In this paper, the empirical equation proposed by Wan et al. [29] is adopted to calculate the wave energy generated by typhoons, but regional water depth is not fully considered. Therefore, future researches should further consider water depth and relevant appropriate wave

calculation equations (for both shallow water and deep water), so as to better simulate the spatial-temporal distribution of typhoon-generated wave energy.

Acknowledgments-The work was financially supported by the National Natural Science Foundation of China (Grant No. 51809047); Fujian Provincial Natural Science Foundation (Grant No. 2019J05029).

REFERENCES

- [1] Lv, C., Liu, S., Wang, S.M., Lan, Y.M., Rao, Y., 2015. Discussion on advances in power generation equipment and technology for marine renewable energy and its issues. *Journal of Hydroelectric Engineering*, 34(2),195-198.
- [2] O'Connor, M., Lewis, T., Dalton, G., 2013. Techno-economic performance of the Pelamis P1 and Wave star at different ratings and various locations in Europe. *Renewable Energy*, 9(50), 889-900. <https://doi.org/10.1016/j.renene.2012.08.009>
- [3] Grunthal, G., Wahlstrom, R., Stromeyer, D., 2013. The SHARE European Earthquake Catalogue (SHEEC) for the time period 1900–2006 and its comparison to the European-Mediterranean Earthquake Catalogue (EMEC). *Journal of Seismology*, 5(10), 1-6 <https://doi.org/10.1007/s10950-013-9379-y>
- [4] Nimmrichter, S., Hornberger, K., Haslinger, P., Arndt, M., 2010. Testing spontaneous localization theories with matter-wave interferometry. *Phys. Rev. A*, 4(83), 36-4 <https://doi.org/10.1103/PhysRevA.83.043621>
- [5] Toshiaki K., 2017. Dream of marine-topia: new technologies to utilize effectively renewable energies at offshore. *Current Applied Physics*, 10(2), 10-23
- [6] Li, J. E., Ding, C. H., Li, F. Z., Lin, W. S., Chen, Y. L., 2014. Overview and prospects for development of wave and offshore wind energy. *Brodogradnja*, 65(2), 79-101.
- [7] Legaz, M. J., Soares, C. G., 2022. Evaluation of various wave energy converters in the bay of Cadiz. *Brodogradnja*, 73(1), 57-88 <https://doi.org/10.21278/brod73104>
- [8] Liu, W. M., Ma, C. L., Chen, F. Y., 2018. Exploitation and Technical Progress of Marine Renewable Energy. *Advances in Marine Science*, 36(1), 1-18.
- [9] van Nieuwkoop, J. C. C., Smith, H. C. M., Smith, G. H., Johanning, L., 2013. Wave resource assessment along the Cornish coast (UK) from a 23-year hindcast dataset validated against buoy measurements. *Renewable Energy*, 58(3), 1-14. <https://doi.org/10.1016/j.renene.2013.02.033>
- [10] Bento, A. R., Martinho, P., Soares, C. G., 2011. Modelling wave energy resources for UK's southwest coast. *2011 Ieee - Oceans Spain*, Santander,Spain. <https://doi.org/10.1109/Oceans-Spain.2011.6003533>
- [11] Rusu, E., Soares, C. G., 2009. Numerical modelling to estimate the spatial distribution of the wave energy in the Portuguese nearshore. *Renewable Energy*, 34(6), 1501-1516. <https://doi.org/10.1016/j.renene.2008.10.027>
- [12] Iglesias, G., Carballo, R., 2010. Offshore and inshore wave energy assessment: Asturias (N Spain). *Energy*, 35(5), 1964-1972. <https://doi.org/10.1016/j.energy.2010.01.011>
- [13] Clement, A., McCullen, P., Falcao, A., 2002. Wave energy in Europe: current status and perspectives. *Renewable and Sustainable Energy Reviews*, 6(5), 405-431. [https://doi.org/10.1016/S1364-0321\(02\)00009-6](https://doi.org/10.1016/S1364-0321(02)00009-6)
- [14] Liu, Q. L., Zhang, Y. L., Liang, S. D., 2015. Numerical study of wave energy resources in Zhaitang Island sea area. *Journal of Hydroelectric Engineering*, 34(11), 148-156.
- [15] Wang, C. K., Shi, W. Y., 2008. Assessment and evaluation of ocean resources in China // Proceedings of 1st Academic Conference of Chinese Renewable Energy Society Ocean Energy Professional Committee. *Ocean Energy Professional Committee of the Chinese Renewable Energy Society*, 8(7), 169-179.
- [16] Zheng, C. W., Zheng, Y. Y., Chen, H. C., 2011. Research on wave energy resources in the Northern South China Sea during recent 10 years using SWAN wave del. *Journal of Subtropical Resources and Environment*, 2(6), 54-59.
- [17] Zhou, K., Wang, R., 2013. Preliminary analysis on wave energy resources in the sea adjacent to Shandong Peninsula. *Water Power*, 11(39), 94-99.
- [18] Ye, Q., Yang, Z. L., Shi, W. Y., 2014. Assessment of China's offshore wave energy resources based on the high-resolution numerical simulation technology. *Journal of Ocean Technology*, 4(33), 117-121.

- [19] Xu, L. D., He, Z. G., Pan, J. J., 2019. Numerical study of wave effects on changes in offshore morphology during storm surges. *Journal of Hydroelectric Engineering*, 38(3), 23-31.
- [20] Chen, W. B., Chen, H. G., Hsiao, S. C., 2019. Wind forcing effect on hindcasting of typhoon-driven extreme waves. *Ocean Engineering*, 188, 106260. <https://doi.org/10.1016/j.oceaneng.2019.106260>
- [21] Hsiao, S. C., Chen, H. G., Chen, W. B., 2019. Quantifying the contribution of nonlinear interactions to storm tide simulations during a super typhoon event. *Ocean Engineering*, 194, 106661. <https://doi.org/10.1016/j.oceaneng.2019.106661>
- [22] Liu, W. C., Huang, W.C., 2020. Investigating typhoon-induced storm surge and waves in the coast of Taiwan using an integrally-coupled tide-surge-wave model. *Ocean Engineering*, 212, 107571. <https://doi.org/10.1016/j.oceaneng.2020.107571>
- [23] Ying, W. M., Zheng, Q., Zhu, C. C., 2017. Numerical simulation of CHAN-HOM typhoon waves using SWAN model. *Marine Sciences*, 41(4), 108-117.
- [24] Chong, W., Pan, J., 2012. Wind Energy Resources Assessment in Global Ocean. *Zheng Journal of Nature Resources*, 27(03), 364-371.
- [25] Zhang, P., Chen, X. L., Lu, J. Z., 2011. Research on wave simulation of Bohai Sea based on the CCMP remotely sensed sea winds. *Marine Science Bulletin*, 30(03), 266-271.
- [26] Yin, J., Dai, E. F., Wu, S. H., 2013. A study on the relationship between typhoon intensity grade and disaster loss in China. *Geographical Research*, 32(2), 266-274.
- [27] Jin, L. B., Chen, G. P., Zhao, H. J., 2015. Study of combined wind in simulating storm waves in the South China Sea. *Journal of Waterway and Harbor*, 36(1), 12-20.
- [28] Zhang, L., She, X. J., Ma, J. R., 2018. Physical experimental study on flow dynamic and sediment of reclamati on plan in Qin Zhou bay. *Journal of Waterway and Harbor*, 39(01), 31-37.
- [29] Hsiao, S. C., Wu, H. L., Chen, W. B., Guo, W. D., Chang, C. H., & Su, W. R., 2021. Effect of Depth-Induced Breaking on Wind Wave Simulations in Shallow Nearshore Waters off Northern Taiwan during the Passage of Two Super Typhoons. *Journal of Marine Science and Engineering*, 9(7), 706. <https://doi.org/10.3390/jmse9070706>
- [30] Wan, Y., Zhang, J., Meng, J. M., 2015. A wave energy resource assessment in the China's seas based on multi-satellite merged radar altimeter data. *Acta Oceanologica Sinica*, 34(03), 115-124. <https://doi.org/10.1007/s13131-015-0627-6>

Submitted: 19.05.2022.

Accepted: 19.09.2022.

Cheng Chen
Chen Peng, 1525246577@qq.com
Hong Xiao
Tingyu Wang
Minjian Wei
College of Civil Engineering, Fuzhou University, Fuzhou, China